Generalized Elastic Lateral-Torsional Buckling of Steel Beams

ROBERT S. GLAUZ and BENJAMIN W. SCHAFER

ABSTRACT

A concise review is provided of the classical elastic lateral-torsional buckling moment for steel beams as utilized in the AISC *Specification* (2022). Rather than make assumptions regarding the cross-section properties, the derivation is provided in its general form for an arbitrary steel beam—that is, one that may be asymmetric and may include any manner of varying geometry, thickness, or cross-section shape. The cross-section properties that underpin the calculation are fully detailed. The assumptions that are inherent in the classical derivations (no shear, no cross-section distortion, etc.) are also fully detailed. The manner in which the generalized lateral-torsional buckling formula may be simplified for particular sections (e.g., a singly symmetric channel) with no loss of accuracy is explained. Adaptations and approximations utilized in the 2022 edition of the AISC *Specification* for elastic lateral-torsional buckling moment of specific sections (e.g., mono-symmetric I-section, angles, etc.) are assessed against the actual elastic solution, and the accuracy and clarity of the assumptions utilized are evaluated. The generalized formula, consistent with current assumptions but applicable to all structural steel cross sections, is recommended for future reference in the main body of the AISC *Specification*.

Keywords: lateral-torsional buckling, elastic buckling, steel beams.

INTRODUCTION

Steel beams with large unbraced spans are susceptible to lateral-torsional buckling. This instability is manifested by simultaneous lateral translation and twisting of the member, as shown in Figure 1. Upon lateral-torsional buckling, the beam is unable to carry additional load due to the formation of plastic mechanisms in the cross section triggered by the buckling that ultimately result in localized loss of stiffness and the potential for collapse. Slender members with narrow cross sections and long unbraced lengths are more susceptible to lateral-torsional buckling.

An early example of lateral-torsional buckling failure, before this mechanism was better understood, was the collapse of the Dee Bridge in Chester, England. Built in 1846 for rail transportation, the main girders were 45 in. deep cast iron with 24-in.-wide bottom flanges but only 7-in.-wide top compression flanges. Lateral-torsional instability (among other factors) led to the collapse during the crossing of a multi-car passenger train in 1847 (Commissioners of Railways, 1848). Bridge engineers learned from this and other failures that the compression flange must be stabilized or increased in size to prevent buckling.

Robert S. Glauz, Owner, RSG Software, Inc., Lee's Summit, Mo. Email: glauz@rsgsoftware.com (corresponding)

Benjamin W. Schafer, Professor, Johns Hopkins University, Baltimore, Md. Email: schafer@jhu.edu

Paper No. 2024–08

The AISC *Specification for Structural Steel Buildings*, hereafter referred to as the AISC *Specification*, has evolved significantly over its history. The first edition (AISC, 1923) protected against lateral-torsional buckling in a simple, but effective and safe manner, treating the compression flange as a column expressing strength as a function of slenderness (L/b), where L is the beam length and b is the compression flange width. Column stability was reasonably well understood based on the early work of Euler (1744), although the mathematics of beam elastic lateral-torsional buckling was not formalized until later by Timoshenko (1936). As shown in Figure 2, the design bending stress F_b was reduced as L/b increased from 15 to an upper limit of 40. This upper limit ensured sufficient stability to prevent elastic buckling failure. The 1936 edition of the AISC *Specification* continued using the same approach, allowing higher stress consistent with the higher yield strength of A9 structural steel at that time.

By the 1946 edition (AISC, 1946), the mechanics of elastic lateral-torsional buckling were better understood. The two components of torsional stiffness for a doubly symmetric I-section can be approximated in terms of $(L/b)^2$ for the warping resistance and Ld/bt for the pure torsion resistance (Salmon and Johnson, 1980). For the vast majority of I-sections used in construction at the time, the flanges were thick enough for the pure torsion resistance to dominate. Therefore, the lateral-torsional buckling design stress changed to a form using slenderness Ld/bt, where d is the depth of the section and t is the thickness of the flange. As shown in Figure 2, this significantly increased the design stress for many I-sections and the upper limit on slenderness was removed.

The 1961 edition (AISC, 1961) continued with the same design stress expression using Ld/bt. Due to the introduction of A36 steel and the availability of different steel grades, this was the first edition to incorporate the material yield strength F_y into the provisions. This edition also recognized that deeper I-sections with thinner flanges could achieve higher strength due to the warping resistance. Therefore, the design stress was permitted to be the larger of the 1946 formula and a new inelastic buckling expression utilizing $(L/r)^2$. Instead of the compression flange width b, this formula used r, defined as the radius of gyration of a tee section comprising the compression flange plus ⅙ of the web area, which is approximately $0.27b$ for a rectangular flange. This generalization accommodated the use of flange geometries other than rectangular. The 1961 edition also included a Commentary that acknowledged the existence of more accurate calculation methods stating: "Rational expressions for the elastic buckling strength of the beam, which take into account its torsional rigidity about its longitudinal axis as well as the bending stiffness of its compression flange, are too complex for general office use." Tables of torsional properties did not appear in the AISC *Steel Construction Manual*, hereafter referred to as the AISC *Manual*, until the eighth edition (AISC, 1981).

It wasn't until the 1986 LRFD edition (AISC, 1986) that both components of torsional stiffness were combined to correctly calculate the critical buckling moment for an I-section, rather than the larger of the two components. As a theoretically accurate calculation, its use was later extended to singly symmetric channel sections and may actually be used for any section bending about an axis of symmetry. This edition also provided approximations to the theoretical solution for other sections that are not symmetrical about the axis of bending. These and other approximations unique to particular cross sections are still in use in the current edition of the AISC *Specification* (2022).

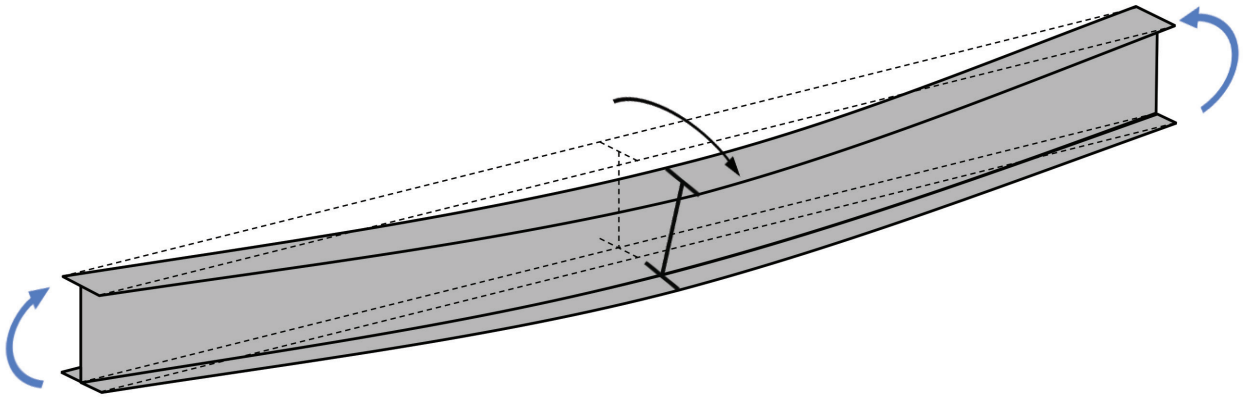

Fig. 1. Lateral-torsional buckling—translation and twist.

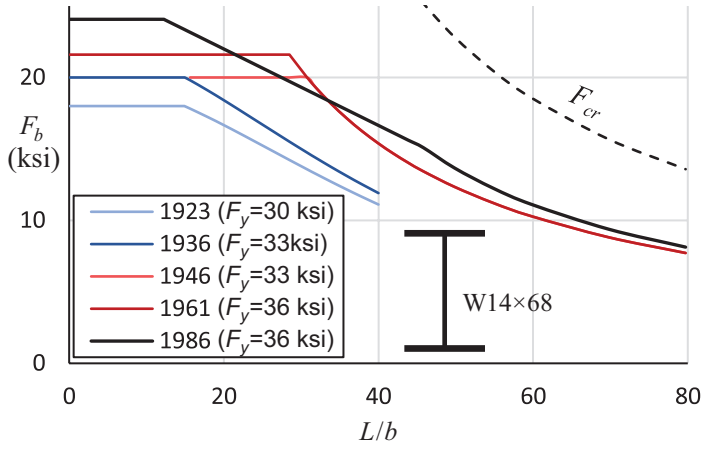

Fig. 2. AISC history of design stress for lateral-torsional buckling.

Figure 2 also illustrates that the 1986 strength permitted moments up to full plasticity, where the allowable design stress is shown as $M_p/1.67S_x$. A new inelastic buckling strength was implemented using a linear transition between the fully plastic moment and the elastic buckling moment.

This paper focuses on determination of the elastic lateral-torsional buckling moment and does not attempt to address inelastic buckling strength. The purpose is to show that the elastic buckling moment calculation can be applied in a consistent way for all cross sections without the approximations that can result in unacceptable error, thus providing a unified approach for all cross sections.

ELASTIC THEORY

The classic approach to the elastic buckling solution of a linear prismatic member is to consider only end forces. The application of axial load P at eccentricities $e_{\dot{x}}$ and $e_{\dot{y}}$ as shown in Figure 3 provides a general solution for a beam-column undergoing any combination of axial load and uniform moments.

Assuming small displacements such that the longitudinal stresses remain constant throughout the member length (first-order analysis), the three equations of equilibrium as expressed by Timoshenko and Gere (1961) are given as:

$$EI_{\dot{y}}\dot{u}^{iv} + P\dot{u}'' + P(\dot{y}_o - e_{\dot{y}})\phi'' = 0 \tag{1}$$

$$EI_{\dot{x}}\dot{v}^{iv} + P\dot{v}'' + P(\dot{x}_o - e_{\dot{x}})\phi'' = 0 \tag{2}$$

$$\begin{aligned} EC_w\phi^{iv} - (GJ - \beta_{\dot{x}}Pe_{\dot{y}} - \beta_{\dot{y}}Pe_{\dot{x}} - Pr_o^2)\phi'' \\ + P(\dot{y}_o - e_{\dot{y}})\dot{u}'' - P(\dot{x}_o - e_{\dot{x}})\dot{v}'' = 0 \end{aligned} \tag{3}$$

where $\dot{x}$ and $\dot{y}$ are the principal axes of the cross section, $\dot{u}$ and $\dot{v}$ are translational displacements in the $\dot{x}$ and $\dot{y}$ directions, ϕ is twisting displacement, E is the modulus of elasticity, G is the shear modulus, and the other variables are geometric properties of the cross section ($I_{\dot{x}}$, $I_{\dot{y}}$, C_w, J, $\dot{x}_o$, $\dot{y}_o$, r_o, $\beta_{\dot{x}}$, $\beta_{\dot{y}}$). To solve these differential equations for warping-free pinned end conditions, the displacements ($\dot{u}$, $\dot{v}$, ϕ) are assigned sinusoidal forms of one half-wavelength, end translation and twist are restrained ($\dot{u} = \dot{v} = \phi = 0$), and end moments and bimoments are zero ($\dot{u}'' = \dot{v}'' = \phi'' = 0$). The result is three simultaneous equations solved by equating the determinant of the coefficients to zero:

$$\begin{bmatrix} P_{e\dot{y}} - P & 0 & -P\dot{y}_o + M_{\dot{x}} \\ 0 & P_{e\dot{x}} - P & P\dot{x}_o - M_{\dot{y}} \\ -P\dot{y}_o + M_{\dot{x}} & P\dot{x}_o - M_{\dot{y}} & (P_t - P)r_o^2 - \beta_{\dot{x}}M_{\dot{x}} - \beta_{\dot{y}}M_{\dot{y}} \end{bmatrix} \begin{Bmatrix} \dot{u} \\ \dot{v} \\ \phi \end{Bmatrix} = \begin{Bmatrix} 0 \\ 0 \\ 0 \end{Bmatrix} \tag{4}$$

where $M_{\dot{x}}$ ($Pe_{\dot{y}}$) and $M_{\dot{y}}$ ($Pe_{\dot{x}}$) are the end moments produced by the axial eccentricities, and $P_{e\dot{x}}$, $P_{e\dot{y}}$, and P_t are the axial loads at which elastic buckling occurs about the $\dot{x}$-axis, about the $\dot{y}$-axis, and in torsion, respectively:

$$P_{e\dot{x}} = \frac{\pi^2 EI_{\dot{x}}}{L^2} \tag{5}$$

$$P_{e\dot{y}} = \frac{\pi^2 EI_{\dot{y}}}{L^2} \tag{6}$$

$$P_t = \frac{1}{r_o^2}\left(GJ + \frac{\pi^2 EC_w}{L^2}\right) \tag{7}$$

The case of interest for lateral-torsional buckling is bending about the major principal axis. Using $\dot{x}$ as the major principal axis, the eccentricity $e_{\dot{y}}$ is increased as the axial load P approaches zero. In the limit, $P = 0$, $M_{\dot{y}} = 0$, and $M_{\dot{x}}$ is the critical moment for buckling about the $\dot{x}$ axis given by the equation:

$$M_{\dot{x}}^2 + \beta_{\dot{x}}P_{e\dot{y}}M_{\dot{x}} - r_o^2P_{e\dot{y}}P_t = 0 \tag{8}$$

The general solution to this quadratic has two roots representing the critical moments for positive and negative bending ($\pm e_{\dot{y}}$). For beams bending about a non-principal x-axis, the elastic lateral-torsional buckling moment is given by the same formula as shown in Glauz (2017), with

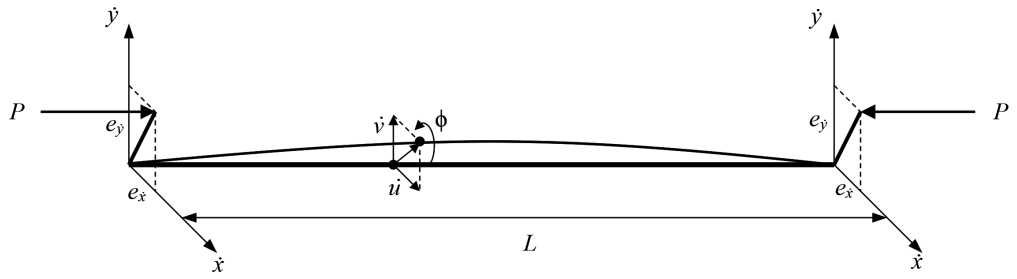

Fig. 3. Beam-column elastic buckling problem.

a more generalized expression for the flexural buckling component.

$$M_x^2 + \beta_x P_{ey} M_x - r_o^2 P_{ey} P_t = 0 \quad (9)$$

$$P_{ey} = \frac{\pi^2 E I_y}{L^2}\left(1 - \frac{I_{xy}^2}{I_x I_y}\right) = \frac{\pi^2 E}{L^2}\left(\frac{I_x I_y - I_{xy}^2}{I_x}\right) = \frac{\pi^2 E I_{\dot{x}} I_{\dot{y}}}{L^2 I_x} \quad (10)$$

where I_x and I_y are the moments of inertia about any orthogonal x- and y-axes (often the geometric axes of the section), and I_{xy} is the product of inertia. As the x-axis approaches the principal $\dot{x}$-axis, the product of inertia I_{xy} approaches zero and P_{ey} becomes $P_{e\dot{y}}$.

OTHER CONSIDERATIONS

The preceding development assumes small displacements and the results agree with numerical elastic buckling analyses based on first-order internal stresses. In reality, displacements prior to buckling (second-order effects) alter the buckling response. For bending about the x-axis, deflection in the y-direction prior to buckling provides a stabilizing effect and enables a higher buckling moment. The closer the ratio I_y/I_x approaches 1, the greater the increase in buckling moment. For $I_y > I_x$, the x-axis is no longer the major axis, and lateral-torsional buckling is unlikely to occur, although still possible for unsymmetrical sections with large β_x magnitude, low torsional stiffness, and shear center in tension.

In addition, the preceding solution assumes no distortion occurs within the cross section as the member undergoes lateral-torsional buckling. If the web is slender enough, destabilization of the flange during lateral-torsional buckling may result in section distortion—often referred to as elastic lateral-distortional buckling (Bradford, 1992). This mode of buckling may be especially likely when bracing is only present for the compression flange and not the full member depth. Further, elastic local plate buckling in the section (another form of potential distortion in the section) and its potential interaction with lateral-torsional buckling are not covered here.

The provided buckling solution assumes warping-free pinned end conditions—that is, translation and twisting are restrained, and rotation and warping are free at both ends. Other end conditions where flexural and twisting wavelengths align will yield the same solution, except with L replaced by the half-wavelength KL, where K is an effective length factor. As an example, fixing the rotation and warping at both ends corresponds to $K = 0.5$. For boundary conditions where flexural and twisting wavelengths do not align, the solution is more complex. However, the critical moment can be approximated using different KL values for the flexural component, P_{ey}, and the torsional component, P_t.

The buckling solution (Equation 8) is also based on a uniform moment induced by equal and opposite end moments. The elastic buckling moment for unequal end moments has historically been handled in the AISC *Specification* by approximation using a multiplicative bending coefficient C_b, based on the ratio of the end moments as given by Equation 11, where M_2 is the larger end moment and the ratio $M_1/M_2 = -1$ for uniform moment.

$$C_b = 1.75 + 1.05\frac{M_1}{M_2} + 0.30\left(\frac{M_1}{M_2}\right)^2 \le 2.3 \quad (11)$$

This C_b coefficient increases the buckling moment by up to 2.3 times the uniform moment case, where the resulting buckling moment is the magnitude at the M_2 end. Further, Equation 11 for C_b assumes a linear moment diagram; however, the primary application for beams involves transverse loading and thus a nonlinear moment diagram (e.g., parabolic for uniform load). Many codes use the refined bending coefficient shown in Equation 12 to more accurately approximate the buckling moment for unbraced spans with transverse loads. It is a slight variation of the expression developed by Kirby and Nethercot (1979), which uses the absolute value of applied moments at the quarter points (M_A, M_B, M_C) and the maximum moment (M_{max}) within the unbraced span. This multiplier ranges from 1.0 to 5.0, and the resulting buckling moment is the magnitude at the location of M_{max}.

$$C_b = \frac{12.5 M_{max}}{2.5 M_{max} + 3 M_A + 4 M_B + 3 M_C} \quad (12)$$

Other bending coefficient expressions have been developed to approximate the buckling moment for some specific cases, such as Wong and Driver (2010) for doubly symmetric I-shape beams, Helwig et al. (1997) for singly symmetric I-shape beams, and Yura (1995) for interior span of I-shape beams with top flange lateral restraint.

The application of transverse loads also produces shear stresses in the member. The elastic buckling solution leading to Equation 8 does not consider shear stresses, which for slender beams are minor compared to longitudinal stresses; however, Liang et al. (2022) have shown cases where shear stresses are important to consider and provided modifications to the classic formula. The location of transverse load application can also influence the lateral-torsional buckling behavior. For a vertical load applied with a horizontal offset from the shear center, torsional forces are applied to the member. The resulting pre-buckling torsional displacements can adversely affect the torsional and flexural components of the lateral-torsional buckling response. For a vertical load applied with a vertical offset from the shear center the load application point can either increase

or decrease the buckling moment. For a downward load applied to a beam above the shear center, small rotation of the member prior to buckling will be amplified by the additional torque induced by the load location and decrease the buckling moment. On the other hand, a downward load applied below the shear center will counteract any small rotation of the member prior to buckling and increase the buckling moment. Some design codes such as Eurocode 3 (CEN, 2005) provide additional coefficients to account for the load height effect, and the AISC *Specification* provides additional references in its Commentary.

All of these considerations are excluded from the formulas presented in this article, except that the commonly used bending moment gradient coefficient C_b is included for consistency and clarity.

SECTION PROPERTIES

The elastic buckling solution is applicable to a member of any cross section. The section properties required to determine the buckling moment about the *x*-axis are the moments of inertia, I_x and I_y, the product of inertia, I_{xy}, the torsional warping constant, C_w, the St. Venant torsional constant, J, the polar radius of gyration about the shear center, r_o, and a unique asymmetry property, β_x. Figure 4 shows a general unsymmetrical cross section with *x*- and *y*-axes passing through the centroid, *c*, along with the location of the shear center, *o*, and asymmetry point, *a*. The centroid is the location where axial loads produce no moments, the shear center is the location where transverse loads produce no torsion, and the asymmetry point is the offset from the shear center that produces torsional geometric stiffness due to flexure. The vector from the shear center to the asymmetry point is half of β, and the component of that vector perpendicular to the *x*-axis is $\beta_x/2$.

Analysis of the longitudinal stresses resulting from compression and flexure require integration over the area of the cross section. These integrations correspond to the familiar terms area, A, moments of inertia about the *x*- and *y*-axes, I_x and I_y, the product of inertia, I_{xy}, the polar moment of inertia about the centroid, I_c, and the radius of gyration about the centroid, r_c. The angle to the principal axes, α, and the principal axis moments of inertia, $I_{\dot{x}}$ and $I_{\dot{y}}$, are also given.

$$A = \int_A dA \tag{13}$$

$$I_x = \int_A y^2\, dA \tag{14}$$

$$I_y = \int_A x^2\, dA \tag{15}$$

$$I_{xy} = \int_A xy\ dA \tag{16}$$

$$I_c = \int_A (x^2 + y^2)\, dA = I_x + I_y \tag{17}$$

$$r_c = \sqrt{I_c/A} = \sqrt{I_x/A + I_y/A} = \sqrt{r_x^2 + r_y^2} \tag{18}$$

$$\alpha = \frac{1}{2}\arctan\frac{-2I_{xy}}{I_x - I_y} \tag{19}$$

$$I_{\dot{x}}, I_{\dot{y}} = \frac{1}{2}(I_x + I_y) \pm \frac{1}{2}\sqrt{(I_x - I_y)^2 + 4I_{xy}^2} \tag{20}$$

Analysis of the stresses resulting from torsion first require determination of the torsion axis, or shear center of the cross section. The shear center is the point (x_o, y_o) in the cross section where an applied shear force in any transverse direction produces no torsion. The polar moment of inertia, I_o, and radius of gyration, r_o, about the shear center are similar to those about the centroid, but greater due to the offset of the shear center. The warping constant, C_w, is a measure of torsional stiffness due to warping, analogous to the moment of inertia, I, and bending stiffness due to flexure. The St. Venant torsional constant, J, is a measure of torsional stiffness due to pure torsion.

The distribution of torsional stresses can be difficult to determine for a general cross section. Numerical methods

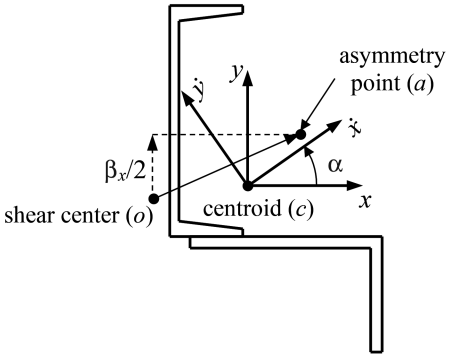

Coordinate Transformations

$$\dot{x} = x\cos\alpha + y\sin\alpha$$
$$\dot{y} = y\cos\alpha - x\sin\alpha$$

$$x = \dot{x}\cos\alpha - \dot{y}\sin\alpha$$
$$y = \dot{y}\cos\alpha + \dot{x}\sin\alpha$$

Fig. 4. Properties of general unsymmetrical cross section.

utilizing finite elements of the cross section are useful for irregular shapes. Computer software is available for this task such as MSASect2 (2023), ShapeBuilder (2023), and Sectionproperties open-source code (2024). For thin-walled open sections, these properties are more readily calculable using sectorial coordinates (ω_c, ω_o, ω_n) and integrating over distance s along the midlines of the cross-section elements of thickness t. These integrations are given as follows:

$$x_o = \frac{I_y \int_0^l \omega_c y t \, ds - I_{xy} \int_0^l \omega_c x t \, ds}{I_x I_y - I_{xy}^2} \tag{21}$$

$$y_o = \frac{I_x \int_0^l \omega_c x t \, ds - I_{xy} \int_0^l \omega_c y t \, ds}{I_x I_y - I_{xy}^2} \tag{22}$$

$$I_o = \int_A \left[(x - x_o)^2 + (y - y_o)^2 \right] dA = I_c + A x_o^2 + A y_o^2 \tag{23}$$

$$r_o = \sqrt{I_o / A} = \sqrt{r_c^2 + x_o^2 + y_o^2} \tag{24}$$

$$C_w = \int_0^l \omega_n^2 t \, ds = \int_0^l \omega_o^2 t \, ds - A \bar{\omega}_o^2 \tag{25}$$

$$\omega_c = \int_0^s \rho_c \, ds \tag{26}$$

$$\omega_o = \int_0^s \rho_o \, ds \tag{27}$$

$$\omega_n = \omega_o - \bar{\omega}_o = \omega_o - \frac{1}{A} \int_0^l \omega_o t \, ds \tag{28}$$

$$J = \frac{1}{3} \int_0^l t^3 \, ds \tag{29}$$

The variables ρ_c and ρ_o are the perpendicular distances to the element midline, measured from the centroid and shear center, respectively. The details of the sectorial coordinate calculations are given in several texts such as Timoshenko and Gere (1961), Yu (2000), and Liu et al. (2018).

Torsional equilibrium given by Equation 3 shows that the coefficient on ϕ'' is the pure torsion elastic stiffness GJ counteracted by the torsion geometric stiffness ($M_{\dot{x}} \beta_{\dot{x}} + M_{\dot{y}} \beta_{\dot{y}} + P r_o^2$), which is produced by the distribution of normal stresses over the cross section resulting from the applied forces $M_{\dot{x}}$, $M_{\dot{y}}$, and P. Based on the work by Glauz (2017), it can be shown that $M_{\dot{x}} \beta_{\dot{x}} + M_{\dot{y}} \beta_{\dot{y}} = M_x \beta_x + M_y \beta_y$; therefore, the β properties associated with the geometric x- and y-axes may be used with the moments about these axes. The properties β_x and β_y are distances given by Equations 30 and 31, equal to twice the orthogonal distances from the shear center (x_o, y_o) to the asymmetry point (x_a, y_a). The coordinates of the asymmetry point are calculated using integrations over the cross-sectional area without the need for thin-walled assumptions.

$$\beta_x = 2(y_a - y_o) \tag{30}$$

$$\beta_y = 2(x_a - x_o) \tag{31}$$

$$y_a = \frac{U_x I_y - U_y I_{xy}}{2(I_x I_y - I_{xy}^2)} \tag{32}$$

$$x_a = \frac{U_y I_x - U_x I_{xy}}{2(I_x I_y - I_{xy}^2)} \tag{33}$$

$$U_x = \int_A y^3 \, dA + \int_A x^2 y \, dA \tag{34}$$

$$U_y = \int_A x^3 \, dA + \int_A y^2 x \, dA \tag{35}$$

For bending about a geometric axis, the properties required to calculate M_{cr} may be calculated using the preceding formulas without transforming coordinates to the principal axes. If the geometric axes are the principal axes, $I_{xy} = 0$ and the formulas for x_o, y_o, x_a, and y_a are simplified. For bending about a principal axis that is not the geometric axis, the necessary section properties may either be calculated as given above and the coordinates x_o, y_o, x_a, and y_a transformed to the rotated principal axes, or all the properties could be calculated using rotated principal axis $\dot{x}$ and $\dot{y}$ coordinates. Note, for a doubly symmetric section, the asymmetry point and the shear center coincide with the centroid, thus all the properties x_o, y_o, x_a, y_a, β_x, and β_y are equal to 0, and the formulas greatly simplify.

APPLICATION

The solution to the quadratic given by Equation 8 is shown below, where M_{cr} is the elastic critical moment about the $\dot{x}$ (major principal)-axis.

$$M_{cr} = C_b P_{e\dot{y}} \left[-\frac{\beta_{\dot{x}}}{2} \pm \sqrt{\left(\frac{\beta_{\dot{x}}}{2} \right)^2 + \frac{r_o^2 P_t}{P_{e\dot{y}}}} \right] \tag{36}$$

An expanded form for M_{cr} is also shown in Equation 37, where P_t and $P_{e\dot{y}}$ have been replaced by their respective expressions.

$$M_{cr} = C_b \frac{\pi^2 E I_{\dot{y}}}{L^2} \left[-\frac{\beta_{\dot{x}}}{2} \pm \sqrt{\left(\frac{\beta_{\dot{x}}}{2} \right)^2 + \frac{GJL^2}{\pi^2 E I_{\dot{y}}} + \frac{C_w}{I_{\dot{y}}}} \right] \tag{37}$$

Equation 36 has the advantage of compactness and commonality with variables used for column buckling; Equation 37 explicitly reveals the influence of unbraced length L and eliminates the r_o property.

Two M_{cr} solutions are given by the positive and negative roots, where the positive root corresponds to a positive moment about the $\dot{x}$ axis—that is, compression on the positive $\dot{y}$ side of the $\dot{x}$-axis ($e_{\dot{y}} > 0$, top flange in compression). Design codes typically provide the magnitude of the buckling moment as a positive number; therefore, the negative root should be negated by multiplying through by –1. This makes the radical additive and changes the sign on the $\beta_{\dot{x}}/2$

term to positive for negative bending. The following form handles this with the C_s sign coefficient having a value of +1 for negative moment ($e_{\dot{y}} < 0$, bottom flange in compression) and −1 for positive moment ($e_{\dot{y}} > 0$, top flange in compression); resulting in:

$$M_{cr} = C_b P_{e\dot{y}} \left[C_s \frac{\beta_{\dot{x}}}{2} + \sqrt{\left(\frac{\beta_{\dot{x}}}{2}\right)^2 + \frac{r_o^2 P_t}{P_{e\dot{y}}}} \right] \tag{38}$$

or

$$M_{cr} = C_b \frac{\pi^2 E I_{\dot{y}}}{L^2} \left[C_s \frac{\beta_{\dot{x}}}{2} + \sqrt{\left(\frac{\beta_{\dot{x}}}{2}\right)^2 + \frac{GJL^2}{\pi^2 E I_{\dot{y}}} + \frac{C_w}{I_{\dot{y}}}} \right] \tag{39}$$

For bending about a non-principal x-axis, the elastic lateral-torsional buckling moment is determined from Equation 9 with P_t and P_{ey} replaced by their expressions from Equations 7 and 10, respectively:

$$M_{cr} = C_b \frac{\pi^2 E (I_x I_y - I_{xy}^2)}{L^2 I_x} \left[C_s \frac{\beta_x}{2} + \sqrt{\left(\frac{\beta_x}{2}\right)^2 + \frac{(GJL^2 + \pi^2 E C_w) I_x}{\pi^2 E (I_x I_y - I_{xy}^2)}} \right] \tag{40}$$

As will be discussed, Equation 40 applies to every cross section utilized in the AISC *Specification*. There is only one formula necessary for predicting the elastic lateral-torsional buckling moment of all steel sections under the assumptions previously stated.

It can be useful to determine the unbraced length L corresponding to any critical moment M_{cr}. Solving Equation 39 (principal axis bending) for L^2 gives the following expression:

$$L^2 = \frac{C_b \pi^2 E I_{\dot{y}}}{M_{cr}} \left[C_s \frac{\beta_{\dot{y}}}{2} + \frac{C_b GJ}{2M_{cr}} + \sqrt{\left(C_s \frac{\beta_{\dot{x}}}{2} + \frac{C_b GJ}{2M_{cr}} \right)^2 + \frac{C_w}{I_{\dot{y}}}} \right] \tag{41}$$

The AISC *Specification* presumes that transitions in strength may occur when M_{cr} reaches a given moment—for example, M_r. Therefore, the length L_r where $M_{cr} = M_r$ may be found by simple substitution into Equation 41:

$$L_r^2 = \frac{C_b \pi^2 E I_{\dot{y}}}{M_r} \left[C_s \frac{\beta_{\dot{y}}}{2} + \frac{C_b GJ}{2M_r} + \sqrt{\left(C_s \frac{\beta_{\dot{x}}}{2} + \frac{C_b GJ}{2M_r} \right)^2 + \frac{C_w}{I_{\dot{y}}}} \right] \tag{42}$$

Calculating M_{cr} requires the section properties $I_{\dot{y}}$, J, C_w, and $\beta_{\dot{x}}$. The $I_{\dot{y}}$ property is readily available for standard shapes and easily calculated for others, whereas the other properties are used less frequently and can be more difficult to calculate. The following subsections discuss these properties for different cases. Formulas are provided for many of these properties using midline dimensions and thin-walled assumptions, ignoring fillets. Full integration including fillets is available in software tools such as those previously mentioned and could be predetermined and tabulated for standard shapes as is done currently for J and C_w in the AISC *Manual* (2023).

Bending about Axis of Symmetry

Figure 5 illustrates several common shapes bending about the axis of symmetry, which is both the geometric x-axis and the principal $\dot{x}$-axis ($I_{xy} = 0$). This symmetry results in $\beta_x = 0$ because the shear center and asymmetry point lie on the axis of symmetry ($y_o = y_a = 0$). The elastic buckling

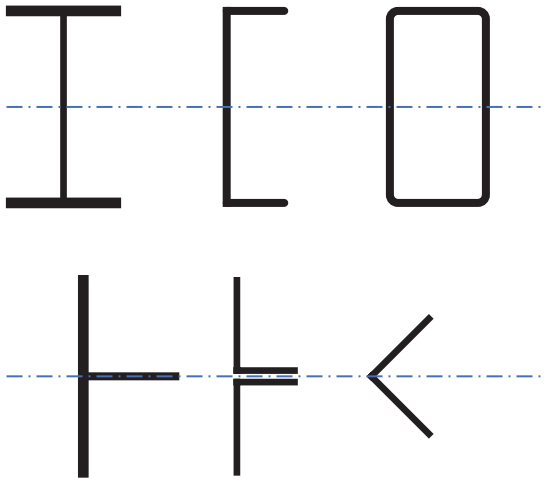

Fig. 5. Sections bending about the axis of symmetry.

equation then simplifies to the following, which is also given in a User Note of the AISC *Specification* (2022) Section F2:

$$M_{cr} = C_b r_o \sqrt{P_{ey} P_t} = C_b \frac{\pi}{L} \sqrt{EI_y \left(GJ + \frac{\pi^2}{L^2} EC_w \right)} \quad (43)$$

For doubly symmetric I-sections (W, M, S, HP) and channels (C, MC), the torsional properties J and C_w are given in AISC *Manual* (2023) tables. For rectangular HSS, tee (WT, MT, ST), double-angle sections, and equal-leg angles, J is given in the AISC *Manual* tables, whereas C_w is much less significant and ignored in the AISC *Specification*. Thick flanges and large fillets increase C_w, which can be computed using numerical methods.

Box Sections

Figure 6 shows a hollow rectangular box section with dimensional parameters and formulas for the required section properties. This section is doubly symmetric, thus $\beta_x = 0$, and Equation 43 is applicable.

Mono-Symmetric I-Section

Figure 7 shows a general mono-symmetric I-section with dimensional parameters and formulas for the required section properties. The C_s sign coefficient corresponds to the direction of the applied moment, but the sign of $\beta_x/2$ is also important and must be calculated properly. The $\beta_x/2$ value is negative when the larger flange is on the positive y-side of the x-axis for I-sections with typical proportions ($t_1 = t_2 > t_w$, $b_2 < b_1 < d_c$).

Tee Section

Figure 8 shows a general tee section with dimensional parameters and formulas for the required section properties. The $\beta_x/2$ value is negative when the flange is on the positive y-side of x-axis for tee sections with typical proportions ($t_1 > t_w$, $b_1 < 2d_c$). The shear center is at the intersection of the flange and web, therefore C_w can be taken as 0.

Double Angle

Back-to-back angle sections are similar to tee sections but with an optional spacing between the vertical legs. Figure 9 shows general back-to-back angles with dimensional parameters and formulas for the required section properties. The $\beta_x/2$ value is negative when the flanges are on the positive y-side of x-axis for typical double angle proportions ($2s_c < b_c < d_c$). The shear center is at the intersection of the flanges and axis between the vertical legs. For close spacings, C_w is small and can be taken as 0.

Single Angle

A common application for a structural angle is loading in the plane of the web with bending about the geometric axis perpendicular to the web. The more general form of the M_{cr} calculation given by Equation 40 is required, which incorporates the term $(I_x I_y - I_{xy}^2)/I_x$ in place of I_y.

Figure 10 shows a general angle section with dimensional parameters and formulas for the required properties, including a direct formula for the expression $(I_x I_y - I_{xy}^2)/I_x$. A simple formula is provided for $\beta_x/2$, which is negative when the flange is on the positive y-side of the x-axis. The shear center is at the intersection of the angle legs; therefore, C_w can be taken as 0 (again assuming mid-line dimensions and thin-walled assumptions, thus ignoring fillets and secondary warping that result in quite small, but non-zero C_w).

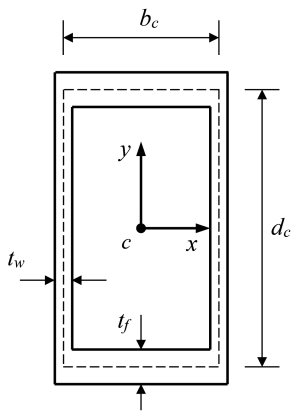

$$A = (b_c + t_w)(d_c + t_f) - (b_c - t_w)(d_c - t_f)$$

$$I_x = \frac{1}{12}(b_c + t_w)(d_c + t_f)^3 - \frac{1}{12}(b_c - t_w)(d_c - t_f)^3$$

$$I_y = \frac{1}{12}(d_c + t_f)(b_c + t_w)^3 - \frac{1}{12}(d_c - t_f)(b_c - t_w)^3$$

$$J = \frac{2b_c^2 d_c^2}{d_c/t_w + b_c/t_f}$$

$$\omega_{n,max} = \frac{b_c d_c (d_c/t_w - b_c/t_f)}{4(d_c/t_w + b_c/t_f)}$$

$$C_w = \frac{1}{3} A \omega_{n,max}^2$$

Fig. 6. Box section properties.

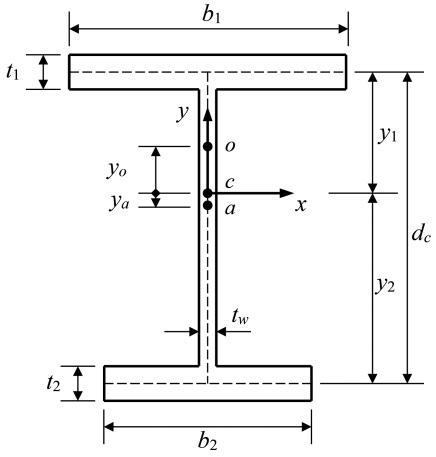

$$A = t_1 b_1 + t_2 b_2 + t_w d_c$$

$$y_1 = (t_2 b_2 d_c + \frac{1}{2} t_w d_c^2)/A \qquad y_2 = d_c - y_1$$

$$I_x = t_1 b_1 y_1^2 + t_2 b_2 y_2^2 + \frac{1}{3} t_w (y_1^3 + y_2^3)$$

$$I_y = \frac{1}{12} t_1 b_1^3 + \frac{1}{12} t_2 b_2^3 = I_{y1} + I_{y2}$$

$$J = \frac{1}{3}(b_1 t_1^3 + b_2 t_2^3 + d_c t_w^3)$$

$$y_o = (t_1 b_1^3 y_1 - t_2 b_2^3 y_2)/12 I_y$$

$$y_a = \begin{bmatrix} t_1 b_1 y_1 (b_1^2 + 12 y_1^2) - t_2 b_2 y_2 (b_2^2 + 12 y_2^2) \\ +3 t_w (y_1^4 - y_2^4) \end{bmatrix} \frac{1}{24 I_x}$$

$$\beta_x / 2 = y_a - y_o$$

$$C_w = t_1 b_1^3 t_2 b_2^3 d_c^2 / 144 I_y = I_{y1} I_{y2} d_c^2 / I_y$$

Fig. 7. Mono-symmetric I-section properties.

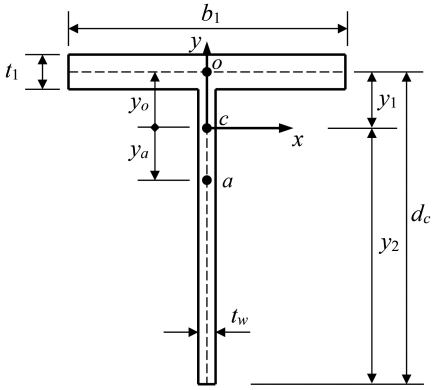

$$y_1 = \frac{t_w d_c^2}{2(t_1 b_1 + t_w d_c)} \qquad y_2 = d_c - y_1$$

$$I_x = t_1 b_1 y_1^2 + \tfrac{1}{3} t_w (y_1^3 + y_2^3)$$

$$I_y = \tfrac{1}{12} t_1 b_1^3$$

$$J = \tfrac{1}{3}(b_1 t_1^3 + d_c t_w^3) \qquad C_w \cong 0$$

$$y_o = y_1$$

$$y_a = \left[t_1 b_1 y_1 (b_1^2 + 12 y_1^2) + 3 t_w (y_1^4 - y_2^4) \right] / 24 I_x$$

$$\beta_x / 2 = y_a - y_o$$

Fig. 8. Tee section properties.

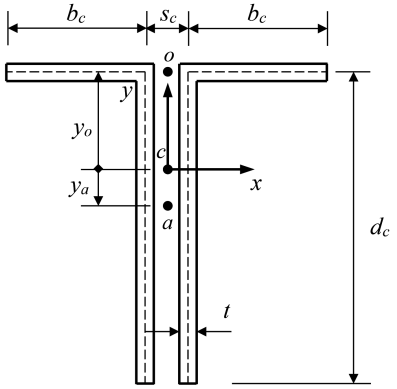

$$I_x = \frac{td_c^3}{6}\left(\frac{4b_c + d_c}{b_c + d_c}\right) \qquad J = \tfrac{2}{3}(b_c + d_c)t^3$$

$$I_y = \frac{t}{6}\left[b_c^3 + 3b_c(s_c + b_c)^2 + 3d_c s_c^2\right]$$

$$y_o = \frac{d_c^2}{2(b_c + d_c)} \qquad C_w \cong 0$$

$$y_a = \frac{b_c^2(2b_c + 3s_c)(b_c + d_c) - 3b_c^2 d_c^2}{2d_c(b_c + d_c)(4b_c + d_c)}$$

$$\frac{\beta_x}{2} = y_a - y_o = \frac{(2b_c^2 - 2b_c d_c - d_c^2)(b_c + d_c) + 3b_c^2 s_c}{2d_c(4b_c + d_c)}$$

Fig. 9. Double-angle section properties.

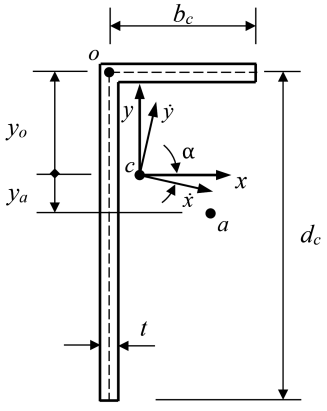

$$I_x = \frac{td_c^3}{12}\left(\frac{4b_c + d_c}{b_c + d_c}\right) \qquad I_{xy} = \frac{tb_c^2 d_c^2}{4(b_c + d_c)}$$

$$I_y = \frac{tb_c^3}{12}\left(\frac{b_c + 4d_c}{b_c + d_c}\right) \qquad J = \tfrac{1}{3}(b_c + d_c)t^3$$

$$\frac{I_x I_y - I_{xy}^2}{I_x} = \frac{tb_c^3}{3}\left(\frac{b_c + d_c}{4b_c + d_c}\right) \qquad C_w \cong 0$$

$$y_o = \frac{d_c^2}{2(b_c + d_c)} \qquad y_a = -\frac{b_c(b_c^2 + 3d_c^2)}{8d_c(b_c + d_c)}$$

$$\frac{\beta_x}{2} = y_a - y_o = -\frac{4d_c^2 - b_c d_c + b_c^2}{8d_c}$$

Fig. 10. Single-angle section properties.

For bending about the principal $\dot{x}$-axis, the properties $I_{\dot{y}}$ and $\beta_{\dot{x}}/2$ are required, which are determined as follows:

$$I_{\dot{y}} = \frac{1}{2}(I_x + I_y) - \frac{1}{2}\sqrt{(I_x - I_y)^2 + 4I_{xy}^2} \tag{44}$$

$$\alpha = \frac{1}{2}\arctan\frac{-2I_{xy}}{I_x - I_y} \tag{45}$$

$$\frac{\beta_{\dot{x}}}{2} = \frac{\beta_x}{2}\cos\alpha - \frac{\beta_y}{2}\sin\alpha = \tag{46}$$
$$-\left(\frac{4d_c^2 - b_c d_c + b_c^2}{8d_c}\right)\cos\alpha - \left(\frac{4b_c^2 - b_c d_c + d_c^2}{8b_c}\right)\sin\alpha$$

For the special case of an equal leg angle, $I_{\dot{y}} = tb_c^3/12$, $\alpha = -\pi/4$, and $\beta_{\dot{x}}/2 = 0$. The major principal axis is an axis of symmetry and the simpler form of Equation 43 can be used.

General Built-Up Section

For any general section built up of other shapes, most section properties can be calculated from the properties of the individual shapes. Figure 11 shows an example built-up section and the method of calculating many of the properties.

Calculating the torsion constant J as the summation of the individual J values is conservative and often accurate enough, but built-up sections that form fully enclosed hollow regions will have much larger J values. This and other torsional properties (shear center and warping constant) are more difficult to calculate for a general section. Software tools that utilize numerical methods are recommended for determining these properties. As with the single angle section, bending about the non-principal x-axis would use Equation 40.

DISCUSSION OF AISC PROVISIONS

The elastic lateral-torsional buckling formulas in the AISC *Specification* (2022) are substantially based on Equation 39; however, many different formulas are given—uniquely customized and approximated for all the different types of standard sections. The accuracy of these elastic buckling formulas and approximations is examined in this section. Note, the objective of the AISC *Specification* is to provide a reliable nominal moment; however, here only the elastic lateral-torsional buckling portion of the calculation is assessed, and thus, the differences do not necessarily equate to meaningful strength reliability and only to accuracy of the elastic expressions.

Bending about Axis of Symmetry

AISC *Specification* Equation F2–4 is shown here as Equation 47 converted from stress to moment, applicable to doubly symmetric I-shapes and channels.

$$M_{cr} = \frac{C_b \pi^2 E S_x}{(L/r_{ts})^2}\sqrt{1 + 0.078\frac{Jc}{S_x h_o}\left(\frac{L}{r_{ts}}\right)^2} \tag{47}$$

$$r_{ts}^2 = \frac{\sqrt{I_y C_w}}{S_x} \tag{48}$$

$$c = 1 \text{ for I-shapes, } c = \frac{h_o}{2}\sqrt{\frac{I_y}{C_w}} \text{ for channels} \tag{49}$$

Equation 47 is identical to Equation 43 but restructured to use new variables r_{ts} and c, which are themselves defined as functions of I_y, C_w, S_x, and h_o. When the expressions for r_{ts} and c are substituted into this equation, the variables S_x

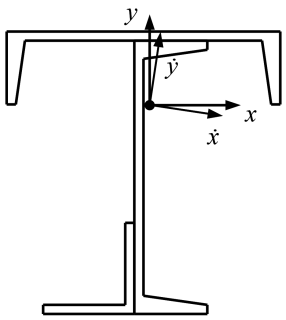

$$I_x = \int_A y^2\,dA = \sum I_{xi} + \sum A_i \bar{y}_i^2$$

$$I_y = \int_A x^2\,dA = \sum I_{yi} + \sum A_i \bar{x}_i^2$$

$$I_{xy} = \int_A xy\,dA = \sum I_{xyi} + \sum A_i \bar{x}_i \bar{y}_i$$

$$J = \sum J_i \quad \text{(conservative)}$$

$$y_a = \frac{U_x I_y - U_y I_{xy}}{2(I_x I_y - I_{xy}^2)}$$

$$U_x = \int_A y^3\,dA + \int_A x^2 y\,dA$$

$$U_y = \int_A x^3\,dA + \int_A y^2 x\,dA$$

Fig. 11. Built-up unsymmetrical section properties.

and h_o factor out entirely. These additional variables are unnecessary and even misleading in suggesting what properties control lateral-torsional buckling. It should also be noted that lateral-torsional buckling for other section types bending about an axis of symmetry as shown in Figure 5 are not addressed in Chapter F.

Mono-Symmetric I-Section

AISC *Specification* Equation F4-5 is shown here as Equation 50 converted from stress to moment, applicable to mono-symmetric I-shapes.

$$M_{cr} = \frac{C_b \pi^2 E S_x}{(L/r_t)^2} \sqrt{1 + 0.078 \frac{J}{S_x h_o} \left(\frac{L}{r_t}\right)^2} \tag{50}$$

This is similar to Equation 47 but restructured to use the additional variable r_t, which is defined as a function of dimensional parameters of the section (i.e., the flange and a portion of the web). The square of r_t is intended to approximate $\sqrt{I_y C_w}/S_x$ combined with the influence of β_x. However, this approximation can lead to significant error compared to Equation 39 as illustrated in Figure 12. The use of r_t (and r_{ts} for doubly symmetric I-shapes) reverts to the pre-1986 concept of treating the compression flange as a column, which is no longer necessary given the availability of the relevant section properties or methods of calculating them. Further, the subtle difference between r_t and r_{ts} can lead to additional error/confusion.

The AISC *Specification* Commentary (2022) includes the theoretically based Equation C-F4-3 incorporating C_w and β_x and is equivalent to Equation 39. An accurate formula for C_w and an approximation for β_x are provided as functions of section depth and flange moments of inertia. Figure 12 shows this approach is more accurate than *Specification* Equation F4-5, although the β_x approximation increases the error for larger flanges.

AISC *Specification* Section F5 also applies to I-shapes but with slender webs. *Specification* Equation F5-4 is shown here as Equation 51, which is the same as Equation 50 with the exclusion of torsional constant J, and is therefore a more conservative approximation of M_{cr}.

$$M_{cr} = \frac{C_b \pi^2 E S_x}{(L/r_t)^2} \tag{51}$$

Square and Rectangular HSS and Box Sections

AISC *Specification* Equation F7-9 is shown here as Equation 52, applicable to closed doubly symmetric rectangular sections—that is, hollow structural sections (HSS) and box sections. This is equivalent to Equation 43 where substitutions have been made for $G = E/2.6$, $I_y = Ar_y^2$, $C_w = 0$, and $\pi/\sqrt{2.6}$ has been rounded up to 2. The assumption that $C_w = 0$ (i.e., negligible) is accurate for square HSS of uniform thickness, although C_w increases with aspect ratio for rectangular HSS. Torsional stiffness is dominated by pure torsion (GJ) for common HSS and box sections; hence, it is generally appropriate to ignore the negligible influence of C_w.

$$M_{cr} = 2EC_b \frac{\sqrt{JA}}{L/r_y} \tag{52}$$

Tees and Double Angles

AISC *Specification* Equation F9-10 is shown here as Equation 53, applicable to tees and double angles. Note that the bending coefficient C_b is not utilized in this equation as explained in the AISC *Specification* Commentary. For these sections, C_w is typically negligible and can be ignored. The new variable, B, in the AISC formula is a dimensionless value intended to represent $(\pi\beta_x/2L)\sqrt{EI_y/GJ}$ by (crudely)

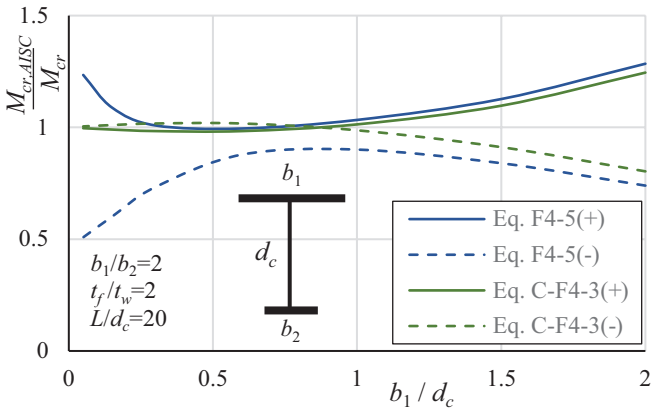

Fig. 12. AISC M_{cr} *equation accuracy for mono-symmetric I-sections.*

approximating β_x as $0.9y_2$. The error introduced by this approximation is shown in Figure 13 for tee sections and Figure 14 for double-angle sections, as compared to Equation 39. For tee sections with $b_1/d_c > 1.5$ and double angles with $b/d > 1$, the error is significant. The error for double angles increases as the spacing between them increases.

$$M_{cr} = \frac{1.95E}{L_b}\sqrt{I_y J}\left(B + \sqrt{1 + B^2}\right) \tag{53}$$

$$B = \pm 2.3\frac{y_2}{L}\sqrt{\frac{I_y}{J}} \tag{54}$$

Single Angle

AISC *Specification* Equation F10-4 is shown here as Equation 55, applicable to single angles bending about their major principal axis. This is equivalent to Equation 39, where substitutions have been made for $G = E/2.6$, $I_{\dot{y}} = Ar_{\dot{y}}^2$, $J = At^2/3$, and $C_w = 0$. Values for $\beta_{\dot{x}}$ are provided in AISC *Specification* Commentary Table C-F10.1 as β_w for common angle sizes independent of thickness. These values are accurate for $b/t = 16$, where b is the longer leg. For b/t other than 16, some small error is introduced.

$$M_{cr} = 1.125\frac{C_b EAr_{\dot{y}}t}{L}\left[\pm 4.4\frac{\beta_{\dot{x}}r_{\dot{y}}}{Lt} + \sqrt{\left(4.4\frac{\beta_{\dot{x}}r_{\dot{y}}}{Lt}\right)^2 + 1}\right] \tag{55}$$

AISC *Specification* Equations F10-5a and 5b are shown here as Equation 56, applicable to equal leg angles bending about the geometric x-axis. This is equivalent to Equation 40, where substitutions have been made for $G = E/2.6$, $(I_xI_y - I_{xy}^2)/I_x = 2tb_c^3/15$, $J = 2b_ct^3/3$, $C_w = 0$, $\beta_x/2 = -b_c/2$, $b = b_c + t/2$, and $t = b/16$. For b/t other than 16, some small error is introduced. AISC *Specification* Section F10 has no provisions for an unequal leg angle bending about a geometric axis.

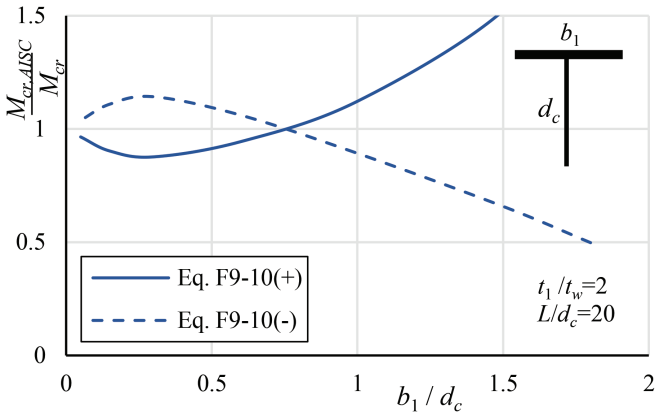

Fig. 13. AISC M_{cr} *equation accuracy for tee sections.*

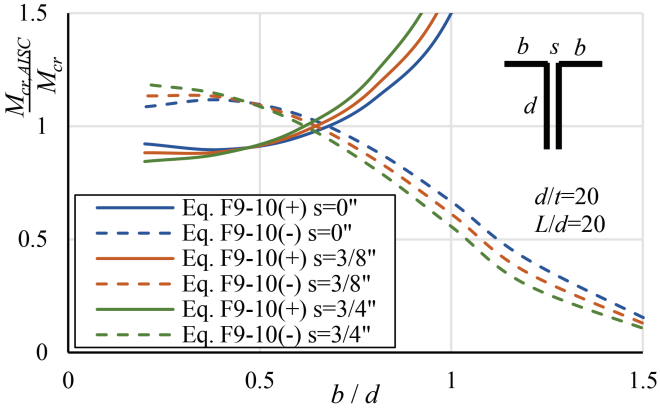

Fig. 14. AISC M_{cr} *equation accuracy for double-angle sections.*

$$M_{cr} = 0.58\frac{C_b E b^4 t}{L^2}\left[\pm 1 + \sqrt{0.88\left(\frac{Lt}{b^2}\right)^2 + 1}\right] \quad (56)$$

Unsymmetrical Sections

AISC *Specification* Section F12 offers no formula to determine M_{cr} for an unsymmetrical section and must therefore be determined by analysis. It is important to note that Equation 40 is valid for unsymmetrical sections, so the task is simply to determine the required properties of the cross section. Although this can be difficult for the torsional properties, section property software tools are available to assist if necessary. Then a more rigorous elastic beam analysis is not necessary.

Recommendations

The AISC *Specification* (2022) presents several different formulas for calculating M_{cr}, with the use of additional variables and approximations. The authors assert that it would be more useful and instructive to provide one general formula to the designer, applicable to any cross section, in the main body of the *Specification*—and provide design aids, or user notes where appropriate, for how the expression simplifies under certain assumptions (cross-section types). Specifically, we recommend that the *Specification* provide Equation 40 for the elastic lateral-torsional buckling moment bending about the geometric x-axis, repeated here for clarity:

$$M_{cr} = C_b \frac{\pi^2 E(I_x I_y - I_{xy}^2)}{L^2 I_x} \left[C_s \frac{\beta_x}{2} + \sqrt{\left(\frac{\beta_x}{2}\right)^2 + \frac{(GJL^2 + \pi^2 E C_w) I_x}{\pi^2 E(I_x I_y - I_{xy}^2)}}\right] \quad (57)$$

For sections where the geometric axes coincide with the principal axes, $I_{xy} = 0$ and the buckling formula can be expressed as:

$$M_{cr} = C_b \frac{\pi^2 E I_y}{L^2}\left[C_s \frac{\beta_x}{2} + \sqrt{\left(\frac{\beta_x}{2}\right)^2 + \frac{GJL^2}{\pi^2 E I_y} + \frac{C_w}{I_y}}\right] \quad (58)$$

If the x-axis is also an axis of symmetry, the shear center and asymmetry point lie on the x-axis ($y_o = y_a = 0$), thus $\beta_x/2 = 0$ and the buckling formula further simplifies to:

$$M_{cr} = C_b \frac{\pi}{L}\sqrt{E I_y\left(GJ + \frac{\pi^2}{L^2} E C_w\right)} \quad (59)$$

The recommendation is to provide Equation 57, along with the simplified formulas for the special cases associated with Equations 58 and 59. For all the common sections covered in AISC *Specification* (2022) Chapter F, closed-form equations have been provided herein for calculating all the necessary section properties (I_x, I_y, I_{xy}, J, C_w, y_o, y_a, $\beta_x/2$), and most of these properties are tabulated in the AISC *Manual* (2023). The addition of $\beta_x/2$ in the torsion property tables would fulfill the section properties requirements. For other sections, formulas can be derived, or software tools utilizing numerical methods may be used.

CONCLUSIONS

The elastic lateral-torsional buckling moment, M_{cr}, for a linear prismatic beam is a single formula applicable to any cross section. Properties of the cross section are required to calculate this buckling moment, including the St. Venant torsional constant, J, and warping constant, C_w. In addition, the less common asymmetry property β_x is required and involves some care in calculation. For sections symmetric about the axis of bending, β_x is zero, and the lateral-torsional buckling moment calculation is greatly simplified.

This article provides formulas for directly calculating β_x for many standard shapes using centerline dimensions and thin-wall assumptions. This includes mono-symmetric I-sections, tee sections, double-angle sections, and single-angle sections. For sections bending about a nonprincipal axis, such as single angles or unsymmetrical built-up sections, the buckling formula is essentially the same except that the minor axis moment of inertia must be generalized to incorporate the product of inertia.

The AISC *Specification* provisions for lateral-torsional buckling consist of different formulas for the various types of standard shapes, where additional variables and formulas are used to approximate β_x rather than calculating the actual values. These approximations introduce errors in the calculation of M_{cr} that can be unacceptably large. The removal of these approximations is recommended. The preferred alternative is to include the β_x property in all the torsional property tables in the next edition of the AISC *Manual*. Such tabulated values could be more accurately determined using direct integration of the cross-section properties to account for fillets and other features not incorporated in the typical mid-line, thin-walled properties. The section property formulas provided herein would also be helpful to include in a future edition of the AISC *Specification* Commentary or the AISC *Manual*.

For unsymmetrical or built-up sections, the calculation of torsional properties and β_x are more difficult. Software tools using numerical methods are available to calculate

these properties. In addition, though not detailed herein, finite element software can be used to model and calculate M_{cr}, not only for unique cross sections, but also for other conditions that affect elastic stability, such as pre-buckling displacements, nonuniform moment, unusual boundary conditions, shear stresses, and load height.

REFERENCES

AISC (1923), *Standard Specification for Structural Steel Buildings*, American Institute of Steel Construction, New York, N.Y.

AISC (1936), *Specification for the Design, Fabrication and Erection of Structural Steel Buildings*, American Institute of Steel Construction, New York, N.Y.

AISC (1946), *Specification for the Design, Fabrication and Erection of Structural Steel Buildings*, American Institute of Steel Construction, New York, N.Y.

AISC (1961), *Specification for the Design, Fabrication and Erection of Structural Steel Buildings*, American Institute of Steel Construction, New York, N.Y.

AISC (1981), *Manual of Steel Construction*, 8th Ed., American Institute of Steel Construction, Chicago, Ill.

AISC (1986), *Specification for Structural Steel Buildings—Load and Resistance Factor Design*, American Institute of Steel Construction, Chicago, Ill.

AISC (2022), *Specification for Structural Steel Buildings*, ANSI/AISC 360–22, American Institute of Steel Construction, Chicago, Ill.

AISC (2023), *Steel Construction Manual*, 16th Ed., American Institute of Steel Construction, Chicago, Ill.

Bradford, M.A. (1992), "Lateral-Distortional Buckling of Steel I-Section Members," *Journal of Constructional Steel Research*, Vol. 23.

CEN (2005), *Eurocode 3: Design of Steel Structures*, EN 1993, The European Committee for Standardization, Brussels, Belgium.

Commissioners of Railways (1848), *Report of the Commissioners of Railways*, London, England.

Euler, L. (1744), *Methodus Inveniendi Lineas Curvas*, Lausannæ & Genevæ, Apud Marcum-Michaelem Bousquet & Socios.

Glauz, R.S. (2017), "Elastic Lateral-Torsional Buckling of General Cold-Formed Steel Beams under Uniform Moment," *Thin-Walled Structures*, Vol. 119.

Helwig, T.A., Frank, K.H., and Yura, J.A. (1997), "Lateral-Torsional Buckling of Singly-Symmetric I-Beams," *Journal of Structural Engineering*, ASCE, Vol. 123.

Kirby, P.A. and Nethercot, D.A. (1979), *Design for Structural Stability*, John Wiley & Sons, Inc., New York, N.Y.

Liang, C., Reichenbach, M.C., Helwig, T.A., Engelhardt, M.D., and Yura, J.A. (2022), "Effects of Shear on the Elastic Lateral Torsional Buckling of Doubly Symmetric I-Beams," *Journal of Structural Engineering*, Vol. 148.

Liu, S.W., Ziemian, R.D., Chen, L., and Chan, S.L. (2018), "Bifurcation and Large-Deflection Analyses of Thin-Walled Beam-Columns with Non-Symmetric Open-Sections," *Thin-Walled Structures*, Vol. 132.

MSASect2 (2023), Matrix Structural Analysis for Arbitrary Cross-Sections, Version 1.0.6, Liu, S.W. and Ziemian, R.D. https://www.github.com/zsulsw/MSASect2.

Salmon, C.G. and Johnson, J.E. (1980), *Steel Structures: Design and Behavior*, 2nd Ed., Harper & Row, New York, N.Y.

ShapeBuilder (2023), Geometric and Structural Properties of Cross Sections, Version 14.0, IES, Inc. https://www.iesweb.com/sb.

Sectionproperties (2024), Open Source Python Package for the Analysis of Arbitrary Cross-Sections Using the Finite Element Method, Version 3.2.1, van Leeuwen, R. https://sectionproperties.readthedocs.io.

Timoshenko, S.P. (1936), *Theory of Elastic Stability*, 1st Ed., McGraw-Hill Book Co., New York, N.Y.

Timoshenko, S.P. and Gere, J.M. (1961), *Theory of Elastic Stability*, 2nd Ed., McGraw-Hill, New York, N.Y.

Wong, E. and Driver, R. (2010), "Critical Evaluation of Equivalent Moment Factor Procedures for Laterally Unsupported Beams," *Engineering Journal*, AISC, Vol. 47, No. 1, pp.1–20.

Yu, W.W. (2000), *Cold-Formed Steel Design*, 3rd Ed., John Wiley & Sons, Inc., New York, N.Y.

Yura, J.A. (1995), "Bracing for Stability—State-of-the-Art," *Proceedings of the ASCE Structures Congress XIII*, Boston, Mass., ASCE, New York, N.Y.